Manipulation of plasmon electron–hole coupling in quasi-free-standing epitaxial graphene layers



2012 New J. Phys. 14 103045

(http://iopscience.iop.org/1367-2630/14/10/103045)

New Journal of Physics
The open-access journal for physics

# Manipulation of plasmon electron–hole coupling in quasi-free-standing epitaxial graphene layers

**Thomas Langer**[1], **Herbert Pfnür**[1], **Christoph Tegenkamp**[1,3], **Stiven Forti**[2], **Konstantin Emtsev**[2] **and Ulrich Starke**[2]

[1] Institut für Festkörperphysik, Leibniz–Universität Hannover, Appelstrasse 2, D-30167 Hannover, Germany
[2] Max-Planck-Institut für Festkörperforschung, Heisenbergstrasse 1, D-70569 Stuttgart, Germany
E-mail: tegenkamp@fkp.uni-hannover.de

*New Journal of Physics* **14** (2012) 103045 (13pp)
Received 1 June 2012
Published 29 October 2012
Online at http://www.njp.org/
doi:10.1088/1367-2630/14/10/103045

**Abstract.** We have investigated the plasmon dispersion in quasi-free-standing monolayer graphene (QFMLG) and epitaxial monolayer graphene (MLG) layers by means of angle resolved electron energy loss spectroscopy. We have shown that various intrinsic p- and n-doping levels in QFMLG and MLG, respectively, do not lead to different overall slopes of the sheet plasmon dispersion, contrary to theoretical predictions. Only the coupling of the plasmon to single particle interband transitions becomes obvious in the plasmon dispersion by characteristic points of inflections, which coincide with the location of the Fermi level above or below the Dirac point. Further evidence is given by thermal treatment of the QFML graphene layer with gradual desorption of intercalated hydrogen, which shifts the chemical potential toward the Dirac point. From a detailed analysis of the plasmon dispersion, we deduce that the interaction strength between the plasmon and the electron–hole pair excitation is increased by about 30% in QFMLG compared to MLG, which is attributed to a modified dielectric environment of the graphene film.

[3] Author to whom any correspondence should be addressed.

## Contents



## 1. Introduction

Two-dimensional (2D) systems, for which graphene is a prototype, cannot exist as isolated objects, but need to be supported or embedded. Inevitably, this embedding into an environment modifies their properties, but at the same time makes these systems even more interesting. Therefore, after the first ground-breaking experiments regarding the mechanical, optical and transport properties in 2D graphene [1–3], many research activities now deal with imperfections and heterogenous environments and how they feed back to those fundamental properties. While short-range order defects are usually rare in epitaxial and exfoliated graphene films, long-range disorder turns out to be an important quantity in this mesoscopic system. For example, the non-vanishing conductivity close to $\approx 4\,e^2/h$ is induced by impurities located at the interface rather than being a universal property of a ballistic system itself [4–6].

A standard way to support graphene films is by their epitaxial growth on metallic and non-metallic substrates. Indeed, graphene films are excellent candidates to study the influence of the interfaces formed. The strength of hybridization between graphene and its support can be tuned by the choice of the substrate. For example, graphene hybridizes strongly with the d-states of Ni(111), while only small charge transfer toward the substrate was found for graphene on Ir(111) [7–9]. Furthermore, the charge transfer may be non-homogeneous across the sample, so that the film is modulated [9]. This modulation, in turn, can be partially lifted by modifying the interface, e.g. by intercalation of Na [10].

For graphene layers grown by sublimation on SiC samples, this strong dependence on interface bonding is even more pronounced. When Si equivalent to three SiC bilayers is evaporated from the Si-terminated SiC(0001) surface, an initial carbon layer—the so-called zero-layer graphene (ZLG)—develops, which forms a $6\sqrt{3} \times 6\sqrt{3})\mathrm{R}30^\circ$ superperiodicity by the epitaxial relationship to the SiC substrate [11, 12]. This layer does not exhibit the linear $\pi$-band dispersion of graphene due to local bond formation at the interface between the $p_z$ orbitals of about one-third of the carbon atoms and unsaturated bonds of the topmost SiC bilayer [13, 14]. The next carbon layer is formed underneath by further Si sublimation from the SiC substrate. It actually assumes the same interface structure, while the former zero-layer converts to epitaxial monolayer graphene (MLG). This layer now has the fully developed $\pi$-band dispersion of graphene, but it is heavily n-doped ($n \approx 10^{13}\,\mathrm{cm}^{-2}$) due to the influence of the interface by its covalent Si–C bonds and the dangling bonds of the remaining unsaturated Si atoms. In contrast, on SiC(000$\bar{1}$) such a buffer layer structure is not formed and it turns

out that the first carbon layer already reveals the full characteristics of a perfect graphene film [15]. On the other hand, the strong coupling of graphene to an SiC(0001) substrate can be lifted by passivating the topmost SiC layer with hydrogen [16–18]. As a result, the original ZLG becomes quasi-free-standing monolayer graphene (QFMLG) so that the strong n-doping, induced by the interface, is compensated or even over-compensated for. For QFMLG, Fermi energies ($E_F$) ranging from 100 to 300 meV below the Dirac point have been reported [16, 19][4].

These strong modifications in epitaxial graphene films have triggered various activities for the studies of quasi-particle dynamics in graphene. As a consequence of the linear band dispersion in a single graphene layer, the group velocities of single particle excitations and other excitations, such as plasmons and phonons, are similar at certain points in phase space. This is a prerequisite for the effective coupling of these excitations so that new quasi-particles are formed. Plasmarons are an example that was studied in detail by angle-resolved photoemission spectroscopy (ARPES) [16, 19–21]. Recently, it was also demonstrated using ARPES data that by modifying the interface with the intercalation of other adsorbates such as fluorine or gold, the coupling strength between the plasmon and the photo-hole can be selectively modified [19]. The different interface termination changes the polarizability of the interface which feeds back to the interaction strength.

Electron loss spectroscopy (EELS) with high momentum resolution has been proven to be a valuable tool to study electronic and vibronic excitations [22, 23]. These can be both single particle or collective excitations. In particular, the properties of collective excitations of the electron gas in low-dimensional systems have been the focus of recent studies [24–27], since several unexpected results were obtained that are not compatible with the standard picture of a quasi-free electron gas. With respect to coupling between single particle and collective excitations, these studies are carried out for the electrically neutral state, so that additional information complementary to that of photoemission is obtained.

In this context, collective excitations in graphene on SiC(0001) have been studied in detail in the past. Most noticeably, the plasmon dispersion curves turn out to be insensitive to the position of the Fermi level, contrary to all standard theories, but reveal a dent, whose minimum coincides with the position of the chemical potential of the graphene film [28, 29]. Adsorption of electronegative F4-TCNQ molecules leads to a shift of this point to lower momentum and lower energy values. This dent in the dispersion can be accurately described within an extended model of the nearly free electron gas by taking into account a momentum (energy)-dependent damping due to excitation of interband electron–hole pairs, which have an increased lifetime [26, 30]. Since this effect depends on the chemical potential, it can be tuned by the interface of the graphene.

This is, in fact, the program realized in this paper. We study the plasmon dispersion of QFMLG, which was prepared by hydrogen intercalation, and prove the consistency of the model put forward in [26]. For the perfect hydrogen intercalated QFMLG, the dispersion shows again the characteristic dent, but at a different position in phase space compared with MLG. By a subsequent annealing of the QFMLG film, the point of inflection can be shifted gradually. This effect is explained fully by our resonance model and the shift of the chemical potential associated with hydrogen desorption.

[4] Depending on the details of the intercalation process the p-doping level can vary by 100 meV. The sample used in this study revealed a Fermi energy of 280 meV below the Dirac point.

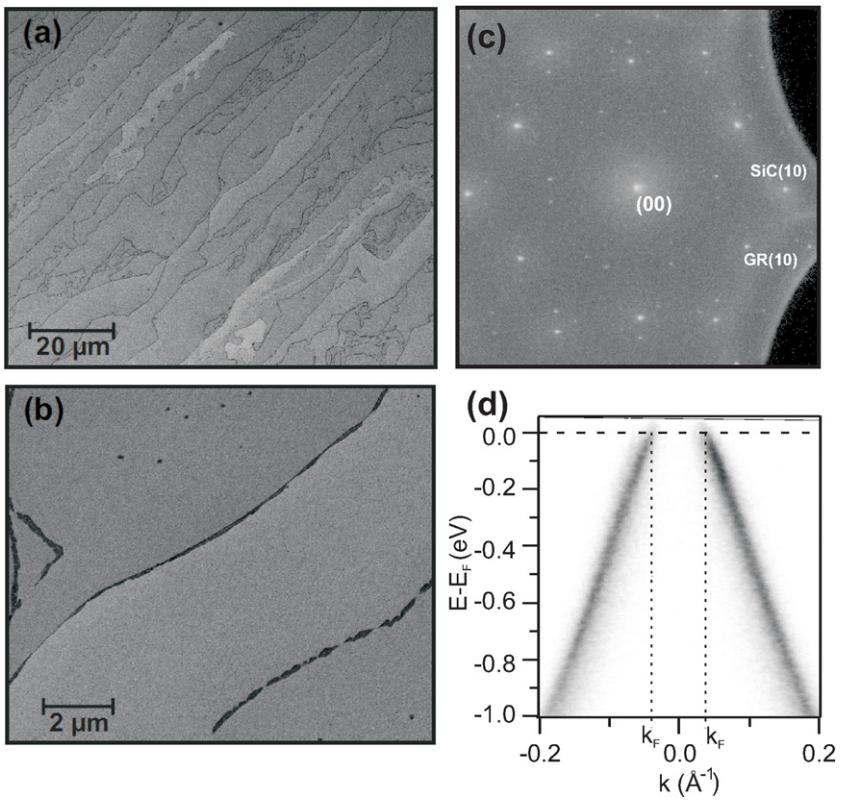


**Figure 1.** SEM (a, b) and LEED image (c) of the QFML graphene grown on 6H-SiC(0001). $HV_{\mathrm{SEM}} = 15\,\mathrm{kV}$ and $E_{\mathrm{LEED}} = 130\,\mathrm{eV}$. The dark lines in (a) and (b) originate from substrate steps of a typical height of one or several SiC unit cell c–vectors ($n \times 1.5\,\mathrm{nm}$). (d) ARPES spectrum ($\pi$-band dispersion around the $k$-point) of the QFMLG film used in this study. Extrapolation reveals a chemical potential of $280 \pm 20\,\mathrm{meV}$ ($k_{\mathrm{F}} = 0.041 \pm 0.002\,\mathrm{Å}^{-1}$, $v_{\mathrm{F}} = 1 \pm 0.1 \times 10^{6}\,\mathrm{m\,s}^{-1}$) below the Dirac point.

## 2. Experimental setup

Single-crystalline 6H-SiC(0001) samples were used as substrate (n-type doping concentration $10^{18}\,\mathrm{cm}^{-3}$), which had been cleaned by wet chemistry and etching in a flow of hydrogen at a temperature of 1400 °C and a pressure of 1 bar in a quartz glass reactor. By this technique residual scratches from polishing steps are effectively removed [31, 32]. As is obvious from figure 1, an atomically flat surface with a very low step density is obtained. The graphitization process was carried out in an argon atmosphere using the same reactor. The initial carbon layer, i.e. ZLG, is formed by annealing the surface for 10 min at 1400 °C [13]. The transformation into a QFMLG film is done in a final step by intercalation of hydrogen at 800 °C close to 1 bar pressure [18]. Both the atomic and the electronic structure for these QFMLG films were controlled by low-energy electron diffraction (LEED), ARPES and scanning electron microscopy (SEM). For further details of the growth process see [16, 18].

The collective modes for these graphene layers were analyzed by means of an angle-resolved electron energy loss spectroscopy LEED system (ELS-LEED) [33]. The measurements

were made under ultra-high vacuum (UHV) conditions ($1 \times 10^{-10}$ mbar). The vacuum system was equipped in addition with a high-resolution spot profile analysis LEED (SPA-LEED) system in order to check the quality of the graphene film on a large scale in reciprocal space. Annealing to 300 °C turned out to be sufficient for complete desorption of the molecules adsorbed during the *ex-situ* transfer of the samples. Typical operating parameters for the ELS-LEED system were 25 meV energy resolution at a $k_{||}$ resolution of $1.3 \times 10^{-2}$ Å$^{-1}$ in the energy range between 15 and 70 eV [33]. By using the SPA-LEED mode of the ELS-LEED instrument, the scattering vector can be accurately measured from the diffraction pattern. The correction factor for the wave vector in the inelastic mode is far below 1% because the loss energies are small compared to the electron energy of the incident beam [33].

## 3. Results and discussion

### *3.1. Plasmons in quasi-free-standing monolayer graphene (QFMLG)*

Using the growth procedure described above, graphene films with a remarkably low defect concentration were obtained. The homogeneity of the SiC sample and the QFMLG on top of it is nicely demonstrated by the SEM images shown in figures 1(a) and (b). The average step spacing is close to 5 $\mu$m. The growth of inhomogeneous multilayer graphene structures on the terraces, which usually takes place for graphene films grown in UHV, is completely suppressed. Only at the very step edge, growth of pristine MLG sets in, which may contribute to the dark stripes seen in the SEM image [16, 34]. The crystallinity of the surface and graphene film was verified by electron diffraction. The SPA-LEED image shown in figure 1(c) shows a perfectly ordered single domain structure. Besides the hexagonally arranged first-order diffraction spots of the substrate, graphene spots are visible as well. The diffracted intensity of the $6\sqrt{3} \times 6\sqrt{3})$R30° reconstruction is strongly reduced in comparison with the ZLG diffraction pattern, i.e. the graphene film is quasi-free standing [16, 18]. Generally, the appearance of bright spots in this superstructure is a clear signature of the strong bonding of the ZLG with the substrate, which induces a severe reconstruction of the carbon layer [13, 14]. The residual faint superstructure spots that are visible in figure 1(c) originate from double diffraction between the QFMLG and the SiC substrate [16]. Nonetheless, even if a small concentration of residual ZLG patches is still present due to an incomplete intercalation, our conclusions regarding collective excitations would not be affected, since these patches are inactive for sheet plasmons. As revealed by ARPES, the QFMLG film is p-doped [16]. The carrier concentrations reported in the literature for H intercalated ZLG samples vary between $2 \times 10^{12}$ and $6 \times 10^{12}$ cm$^{-2}$ corresponding to Fermi energies $E_F$ of approximately 180–300 meV below the Dirac point $E_D$ [17, 35] (see footnote 4), respectively, in contrast to the n-doped MLG on top of a ZLG [18]. In this study, the $E_F$ of the QFMLG is estimated from ARPES to be $280 \pm 20$ meV below $E_D$. The corresponding ARPES spectrum is shown in figure 1(d). A model to explain the origin of this hole concentration in QFMLG has been recently proposed in terms of a spontaneous polarization of the substrate [35]. As we will show in the following, the type and the concentration of doping is reflected very well by plasmon spectroscopy.

Plasmon loss spectra were taken along different directions in $k$-space. Exemplarily, the loss spectra taken at 20 eV primary electron energy measured along the $\overline{\Gamma}$– $\overline{\mathrm{K}}$ direction up to 0.2 Å$^{-1}$ are shown in figure 2. Besides the elastic peak, the spectra are dominated by several characteristic losses. The individual losses and the Drude background were modeled using

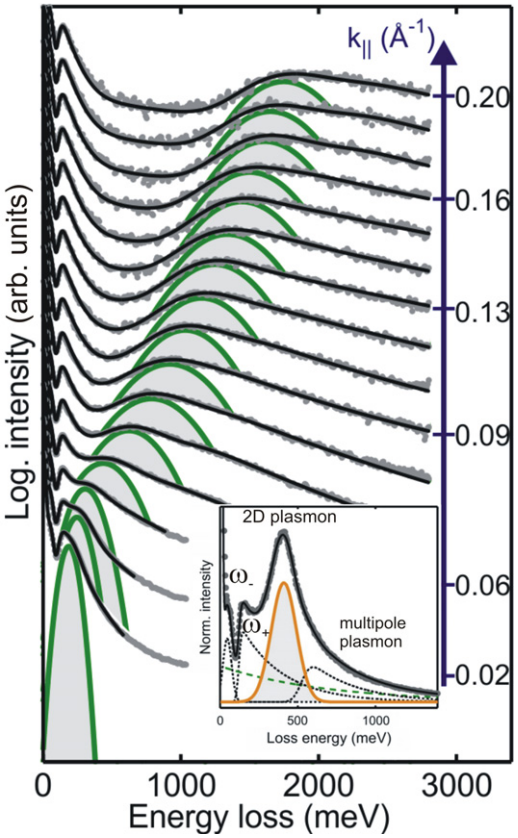


**Figure 2.** Plasmon loss spectra for different $k$-values of QFMLG. Only the 2D plasmon loss peak is highlighted. The primary electron energy was 20 eV. The inset (MLG, linear $y$-scale, $k_{\|} = 0.06\,\text{Å}^{-1}$) shows details of the fitting procedure and labels the dominant loss features. For further information see [28]. All EELS measurements were carried out at room temperature. The dashed (green) line in the inset denotes the Drude background.

(exponentially modified) Gaussian and exponential functions, respectively. As shown in detail in the inset of figure 2, at low loss energies phonon–plasmon polariton states ($\omega_-$, $\omega_+$) are visible [36], which exhibit negligible dispersion in the considered momentum range. The most intense loss peak in the spectrum can be assigned to the 2D plasmon itself, which will be in the focus of this study (see below). It should be mentioned that a further loss peak structure (labeled as multipole plasmon in the inset) is needed in order to model the entire energy loss spectrum consistently. While on SiC substrates this higher-order loss structure has low intensity, for graphene grown on Ir(111) this loss peak was clearly resolved [10] and assigned to a multipole plasmon loss, since it is conceptually similar to the multipole surface plasmons (also called out-of-phase plasmons) found in thin metallic adlayers [27, 37]. In order to compare spectra taken on different samples the same fitting models were applied. Details of the fitting procedure are described in [28]. In general, the dominant energy loss peak position of the sheet plasmon, which is discussed here, is a robust quantity and is rather insensitive to small variations of the fitting procedure.

The resulting dispersion for QFMLG, i.e. the energy position of the 2D plasmon mode versus the momentum, is plotted in figure 3. For comparison also the plasmon mode obtained

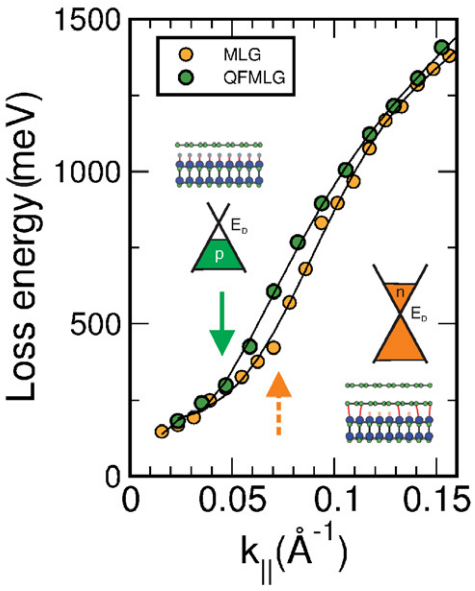


**Figure 3.** Dispersion of the plasmon measured for QFMLG (green circles). The $\pi$-band filling is sketched in green together with a structural sketch. The orange circles represent the dispersion for the plasmon on n-doped MLG [26]. For the respective $\pi$-band filling (orange sketch) and a schematic model, see lower right. The arrows mark the points of inflection for both samples types, which is clearly different between QFMLG (p-doped) and MLG (n-doped). The lines represent fits according to the model described in [26].

for MLG is shown in order to visualize the difference between both dispersions [26, 28]. While the dispersion for plasmons in the long- and short-wavelength regimes is almost identical for QFMLG and MLG, there is a clear difference in the intermediate momentum regime. Contrary to the behavior predicted by theory [30, 38], with an $E \propto \sqrt{k_\parallel}$ behavior at low $k_\parallel$, we always observe a dent in the dispersion curves. The points of inflection are marked by arrows in figure 3, and have been interpreted as being due to the resonance occurring by the opening of the interband decay channel for the plasmons [26]. Compared to the MLG this point is shifted to significantly lower $k$-values in QFMLG with a corresponding energy around 300 meV. This energy coincides with the position of the chemical potential of p-doped QFMLG with respect to the Dirac point [18]. The general trend of the dispersion can still be satisfactorily described by an extended nearly free electron gas model including explicitly the resonant decay channel, i.e. the coupling of the plasmon to long-lived electron–hole pairs. For MLG we have shown recently that this point coincides nicely with the chemical potential of the graphene film of about 500 meV. Details are reported in [26]. In the case when the coupling strength to the environment as well as the n-doping and p-doping levels are the same with respect to the Dirac point, identical plasmon dispersions are expected over the entire range of momentum. It should be mentioned that our semiclassical model can only motivate the existence of a (resonant) decay channel for plasmons. The identification of this channel in the form of an electron–hole excitation is drawn from the coincidence of the loss energy with the chemical potential of the graphene film and

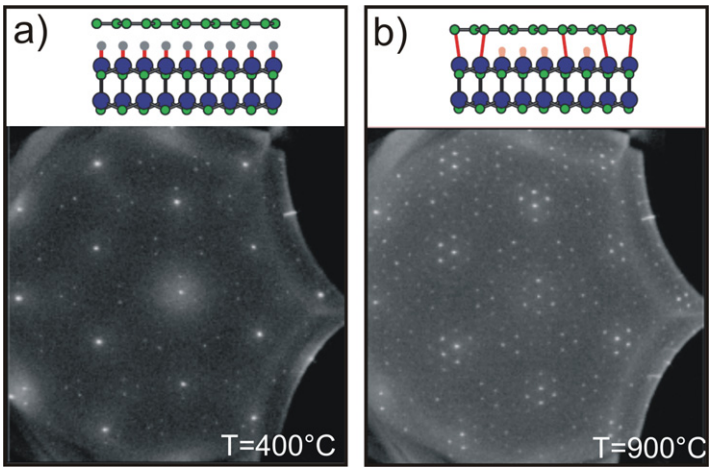


**Figure 4.** LEED patterns of the QFMLG after annealing to (a) 400 °C and (b) 900 °C. The electron energy was 150 eV. After annealing to 900 °C (b), the intercalated hydrogen is fully desorbed and the free-standing graphene layer is transformed into ZLG (buffer layer). The measurements were made at room temperature.

the analogy to ARPES experiments [19]. In order to have further evidence for our model, self-consistent methods including life time effects are needed to put a final word on this subject.

We want to emphasize that the QFMLG films investigated here are extremely smooth. From the ARPES characterization we can safely conclude that the fraction of (quasi-free) bilayer graphene is far below 5%, as also revealed by *ex-situ* Raman measurements. In addition, such bilayer inclusions are restricted to the substrate step regions known from previous low-energy electron microscopy investigations [16], while on the terraces the defect density in the graphene lattice is low, as seen in the SEM image in figure 2(b). Thus, the roughness claimed by Shin *et al* [39] can not be responsible for the dent and its shift. On the other hand, if this effect were based on plasmon–phonon coupling, the point of inflection should appear at lower loss energies for high chemical potentials (compare with [40]), so this origin can also be ruled out. As we demonstrate in the next section, the position of the dent is directly coupled with the position of the chemical potential, which in this study is determined solely by the interface properties.

### *3.2. Thermal treatment of QFML graphene*

In order to demonstrate the role of the Fermi energy ($E_F$) in our plasmon dispersion, the QFML graphene film was subsequently annealed. In recent high-resolution ARPES measurements it was shown that $E_F$ in QFMLG can be tuned by annealing of the film. By partial desorption of the individual hydrogen atoms at temperatures in the range around 700 °C [16], the spontaneous polarization of the underlying substrate is gradually compensated for [35], so that neutral graphene layers are formed. The entire hydrogen can be desorbed at temperatures about 900 °C, leading to a reversal of the decoupling. The complete structural reversal back to the buffer layer (ZLG) is demonstrated with SPA-LEED in figure 4 after different steps of annealing. The pattern corresponding to the $6\sqrt{3} \times 6\sqrt{3})$R30° reconstruction becomes much more intense after high-temperature annealing. As supported also by EELS (see below), the intermediate H-layer

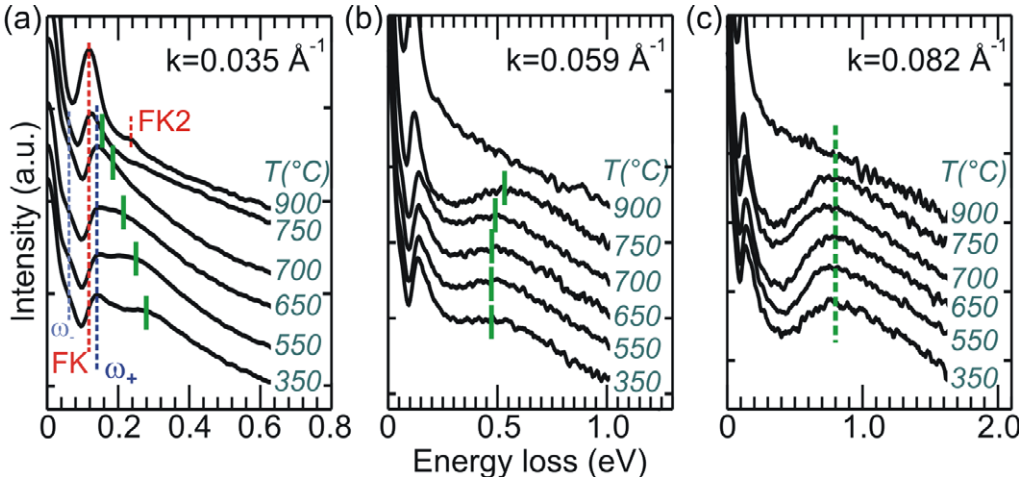


**Figure 5.** (a)–(c) Energy loss spectra taken at three different $k$-values after different steps of annealing. The measurements were made at room temperature. Annealing to 900 °C leads to full desorption of H and the formation of ZLG. The annealing has been performed in front of the ELS-LEED instrument; thus the shift of the plasmon peak is unambiguously related to modifications of the graphene film. The magnitude and direction of the shifts are explained in the context of figure 6.

is fully desorbed after the 900 °C annealing step and an electrically inactive ZLG film without plasmonic losses remains.

The corresponding development of the electronic structure during the process of hydrogen desorption was monitored with EELS. Spectra obtained after subsequent annealing steps are shown for three distinct scattering conditions in figure 5. The dispersion curves, as expected from all previous measurements and from our model, show only small changes. Starting with the plasmon losses recorded at $k = 0.035\,\text{Å}^{-1}$, the main plasmon loss shifts to lower energies (marked by green lines). However, while for large $k$-values (compare with figure 5(c)) the loss peak remains constant, at intermediate $k$-values (figure 5(b)) the loss shifts even to higher energies for annealing temperatures up to 750 °C. Irrespective of the scattering condition the plasmon loss feature disappears completely after heating the sample to 900 °C, demonstrating that the buffer layer has no $\pi$-bands in agreement with photoemission data. Furthermore, the plasmon-induced $\omega_\pm$ states disappear, and the Fuchs–Kliever (FK) mode of the substrate (and even its second harmonic, FK2) reappears (see red dashed lines in figure 5(a)). We would like to point out that the sample geometry was kept fixed during the annealing; thus the changes of the loss profiles are unambiguously related to changes of the graphene film. The shifts of the peaks are directly obvious and are not dependent on details of the fitting routines used. As is obvious from figure 5 the intensities of the plasmon losses remain almost constant irrespective of the annealing temperature. This points toward a homogeneous desorption of hydrogen from the QFML phase rather than desorption from edges resulting in the formation of larger patches of ZLG. Even though details of the hydrogen desorption remain unclear at moment, the results from EELS and ARPES strongly suggest a gradual change of the chemical potential of the entire surface.

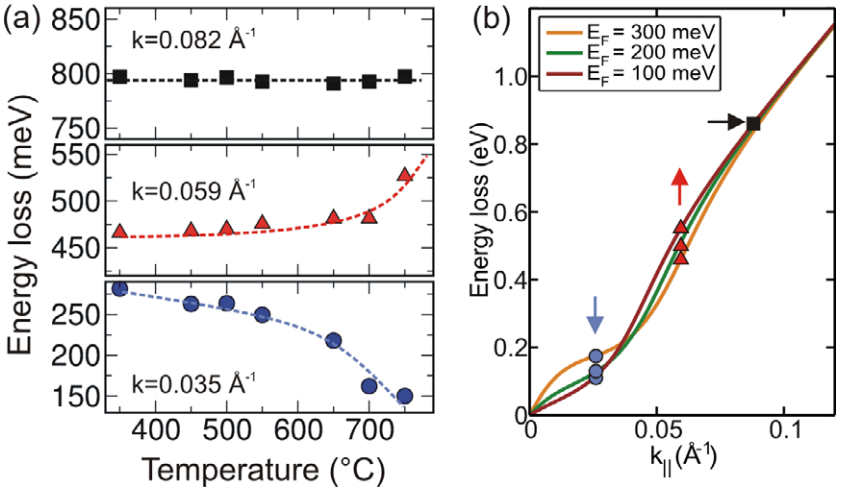


**Figure 6.** (a) Loss energies for the plasmon loss for three scattering conditions as a function of the annealing temperature. The positions were deduced from the spectra shown in figure 5. (b) Plasmon electron–hole dispersion curves plotted exemplarily for three different chemical potentials. Depending on the $k$-vector the loss energies shift to higher/lower values or remain almost constant. The trend is indicated by the arrows. The scattering vectors shown in (a) are marked by symbols.

While at the low $k_{\|}$ values the losses shift to lower energies (compare with figure 5(a)), as predicted by random phase approximation (RPA)-based theory [38], our findings strongly contradict this theory at high $k$-values and, in particular, for scattering conditions in the vicinity of the pristine point of inflection, i.e. at $k \approx 0.05\,\text{Å}^{-1}$, where a shift to higher plasmon loss energies can be seen (figure 5(b)). The effect of the shift of the plasmon mode is obviously related to the chemical potential of the graphene film, which changes upon the annealing steps and which can be explained in the framework of our plasmon electron–hole resonance model (see below). Qualitatively, the results are similar to those obtained by adsorption of F4-TCNQ on MLG [26]. However, by annealing of QFMLG we do not generate additional loss channels due to plasmon scattering at adatoms. Thus broadening of the loss spectra due to scattering of plasmons at adatoms, molecules, etc does not occur [10, 28].

The $k$-dependent shifts of the plasmon loss found in figures 5(a)–(c) are summarized in figure 6(a). The trend seen can be easily rationalized by our plasmon electron–hole resonance model [26]. Using this model, we calculated the expected plasmon dispersion curves for different chemical potentials with respect to the Dirac point. The results are shown in figure 6(b). As a consequence of the S-type dispersion relation, the sign of the relative changes of the plasmon energy depends sensitively on $E_{\text{F}}$ and on $k_{\|}$. For the qualitative modeling we assume that the strength of the resonant damping is the same irrespective of the chemical potential. The trend seen in the experiment, i.e. shift to lower (higher) loss energies at small (intermediate) $k$-values, can be reasonably explained by this simple model. It clearly demonstrates that the origin of the point of inflection is rather induced by an intrinsic graphene property than, e.g., by roughening of the surface, in agreement with the finding that the full width at half maximum (FWHM) of the (00)-LEED spot is unchanged upon the annealing process (cf figure 4).

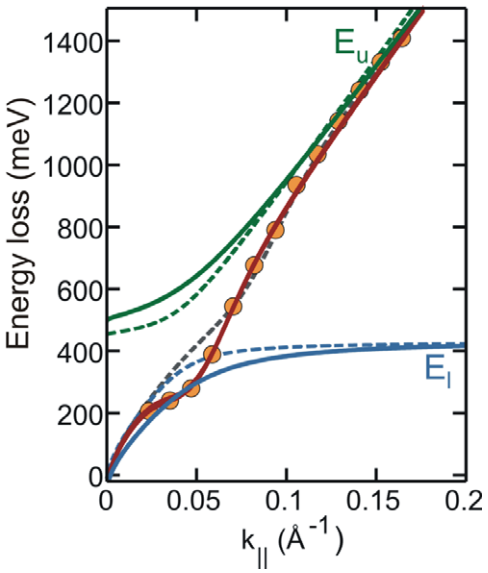


**Figure 7.** Experimental plasmon loss dispersion data (circles) of the QFMLG layer and fitted dispersion curve using the model of two strongly coupled oscillators, as described in detail in [26]. The dashed lines are the best fits obtained for MLG. The coupling strength deduced from the fitting is 30% higher compared to the strength found in MLG.

As mentioned, due to the very short lifetimes of both quasi-particles, i.e. plasmon and electron–hole pairs, the interaction time between both is limited, i.e. instead of a bimodal dispersion, as shown by the $E_u$ and $E_l$-branches in figure 7, the resonance effect is seen only by a red-shift in the plasmon dispersion. Nonetheless, as elaborated in detail in [26], the model for strongly coupled plasmon electron–hole quasi-particles can be used in order to model the regime of short and long wavelengths and to estimate the interaction strength of the quasi-particles. For MLG films grown on ZLG films a coupling strength of $2\Delta = 100$ meV has been deduced [26]. A best fit for the QFMLG film, as shown in figure 7, was obtained assuming a Fermi energy of 300 meV, in agreement with ARPES (cf figure 1(d)). Interestingly, the interaction strength, which is to first order the difference between the upper ($E_u$) and lower ($E_l$) polariton branches around the point of inflection, is increased for the hydrogen intercalated layer by about 30% ($2\Delta = 130$ meV). This finding is in quantitative agreement with recent ARPES studies of plasmon–hole coupling giving rise to plasmaron quasi-particles [19, 21]. In these studies, it was shown that the coupling strength between holes and plasmons can be tuned by changing the effective screening, i.e. it depends on the dielectric environment of the graphene sheet. In particular, QFMLG layers obtained by H- and F-intercalation of ZLG and heavily doped in addition by deposition of potassium have shown a larger energy splitting in the spectral function compared to MLG layers. In this study, where H-atoms at the interface are partially desorbed by thermal treatment, the polarizability and, therefore, the coupling strength between the plasmons and electron–hole pairs changes gradually.

## 4. Summary and conclusion

In this paper, we have analyzed the plasmon dispersion in QFMLG films and compared our results to those obtained for MLG. Both systems reveal in their dispersion points of inflection,

which directly reflect the position of $E_F$. Furthermore, by subsequent annealing of the QFMLG film the chemical potential is shifted toward the Dirac point. The changes seen in the plasmon dispersion at different $k$-values can be reasonably explained by a recently proposed plasmon electron–hole resonance model. For the H-intercalated QFMLG film, the resonance effects appear more pronounced than for MLG due to an increased interaction between plasmon and electron–hole particles.

We point out that our experimental dispersion curves cannot be reproduced by theory so far, in particular its insensitivity to the position of $E_F$ at high $k_\parallel$. Also the dent is not reproduced, possibly because lifetime effects are not considered properly. Nonetheless, qualitative features in this direction, i.e. a point of inflection, can be obtained also on the RPA level if plasmon–phonon coupling [40] or plasmon–plasmon coupling in bilayer systems [41] are taken into account.

We also demonstrate here that neither roughness nor the formation of a multilayer graphene structure is responsible for the behavior of dispersion [28], contrary to recent allegations [39]. Furthermore, plasmon–phonon coupling cannot explain our findings either, as in our case the position of the point of inflection coincides with the Fermi energy in graphene. If phonon–plasmon interaction is dominant, the point of inflection should appear for highly doped graphene films ($10^{13}\,\mathrm{cm}^{-2}$) at lower energies [40]. The systematic study of the plasmon on various substrates clearly suggests that details of the dispersion are related to the Fermi energy of the graphene film, i.e. to the interface of the graphene film.

## Acknowledgments

We gratefully acknowledge financial support for this work from the German Research Foundation (DFG) in the framework of the Priority Program 1459 ‘Graphene’.

## References

[1] Novoselov K S, Geim A K, Morosov S V, Jiang D, Katsnelson M I, Grigorieva I V, Dubonos S V and Firsov A A 2005 *Nature* **438** 197
[2] Zhang Y, Tan Y-W, Stormer H L and Kim P 2005 *Nature* **438** 201
[3] Berger C *et al* 2006 *Science* **312** 1191
[4] Chen J H, Jang C, Adam S, Fuhrer M S, Williams E D and Ishigami M 2008 *Nature Phys.* **4** 377
[5] Das Sarma S, Adam S, Hwang E H and Rossi E 2011 *Rev. Mod. Phys.* **83** 407
[6] Yan J and Fuhrer M S 2011 *Phys. Rev. Lett.* **107** 206601
[7] Popova A, Shikin A, Rybkin A, Marchenko D, Vilkov O, Makarova A, Varykhalov A and Rader O 2011 *Phys. Solid State* **53** 2539
[8] Vanin M, Mortensen J J, Kelkkanen A K, Garcia-Lastra J M, Thygesen K S and Jacobsen K W 2010 *Phys. Rev.* B **81** 081408
[9] Busse C *et al* 2011 *Phys. Rev. Lett.* **107** 036101
[10] Langer T, Förster D F, Busse C, Michely T, Pfnür H and Tegenkamp C 2011 *New J. Phys.* **13** 053006
[11] Starke U and Riedl C 2009 *J. Phys.: Condens. Matter* **21** 134016
[12] Riedl C, Starke U, Bernhardt J, Franke M and Heinz K 2007 *Phys. Rev.* B **76** 245406
[13] Emtsev K V, Speck F, Seyller Th, Ley L and Riley J D 2008 *Phys. Rev.* B **77** 155303
[14] Riedl C, Coletti C and Starke U 2010 *J. Phys. D: Appl. Phys.* **43** 374009
[15] Johansson L I, Watcharinyanon S, Zakharov A A, Iakimov T, Yakimova R and Virojanadara C 2011 *Phys. Rev.* B **84** 125405

[16] Forti S, Emtsev K V, Coletti C, Zakharov A A, Riedl C and Starke U 2011 *Phys. Rev.* B **84** 125449
[17] Speck F, Jobst J, Fromm F, Ostler M, Waldmann D, Hundhausen M, Weber H B and Seyller Th 2011 *Appl. Phys. Lett.* **99** 122106
[18] Riedl C, Coletti C, Iwasaki T, Zakharov A A and Starke U 2009 *Phys. Rev. Lett.* **103** 246804
[19] Walter A *et al* 2011 *Phys. Rev.* B **84** 085410
[20] Bostwick A, Ohta T, Seyller Th, Horn K and Rotenberg E 2007 *Nature Phys.* **3** 36
[21] Bostwick A, Speck F, Seyller T, Horn K, Polini M, Asgari R, MacDonald A H and Rotenberg E 2010 *Science* **328** 999
[22] Rocca M 1995 *Surf. Sci. Rep.* **22** 1
[23] Nagao T, Yaginuma S, Inaoka T, Sakura T and Jeon D 2007 *J. Phys. Soc. Japan* **76** 114714
[24] Diaconesu B *et al* 2007 *Nature* **448** 57
[25] Block T, Baringhaus J, Tegenkamp C, Inaoka T and Pfnür H 2011 *Phys. Rev.* B **84** 205402
[26] Tegenkamp C, Pfnür H, Langer T, Baringhaus J and Schumacher H W 2011 *J. Phys.: Condens. Matter* **23** 012001
[27] Pfnür H, Langer T, Baringhaus J and Tegenkamp C 2011 *J. Phys.: Condens. Matter* **23** 112204
[28] Langer T, Baringhaus J, Pfnür H, Schumacher H W and Tegenkamp C 2010 *New J. Phys.* **12** 033017
[29] Liu Y, Willis R F, Emtsev K V and Seyller Th 2008 *Phys. Rev.* B **78** 201403
[30] Stern F 1967 *Phys. Rev. Lett.* **18** 546
[31] Soubatch S, Saddow S E, Rao S P, Lee W Y, Konuma M and Starke U 2005 *Mater. Sci. Forum* **483–485** 761
[32] Frewin C L, Coletti C, Riedl C, Starke U and Saddow S E 2009 *Mater. Sci. Forum* **615–617** 589
[33] Claus H, Büssenschütt A and Henzler M 1992 *Rev. Sci. Instrum.* **4** 2195
[34] Emtsev K V *et al* 2009 *Nature Mater.* **8** 203
[35] Ristein J, Mammadov S and Seyller T 2012 *Phys. Rev. Lett.* **108** 246104
[36] Koch R J, Haensel T, Ahmed S I-U, Seyller Th and Schaefer J A 2010 *Phys. Status Solidi* c **7** 394
[37] Quinn J 1992 *Solid State Commun.* **84** 139
[38] Hwang E H and Das Sarma S 2007 *Phys. Rev.* B **75** 205418
[39] Shin S Y, Hwang C G, Sung S J, Kim N D, Kim H S and Chung J W 2011 *Phys. Rev.* B **83** 161403
[40] Hwang E H, Sensarma R and Das Sarma S 2010 *Phys. Rev.* B **82** 195406
[41] Hwang E H and Das Sarma S 2009 *Phys. Rev.* B **80** 205405